Electronic structure modification of the $KTaO_3$ single-crystal surface by Ar^+ bombardment

Neha Wadehra,[1] Ruchi Tomar,[1] Soumyadip Halder,[2] Minaxi Sharma,[2] Inderjit Singh,[2] Nityasagar Jena,[1] Bhanu Prakash,[1] Abir De Sarkar,[1] Chandan Bera,[1] Ananth Venkatesan,[2] and S. Chakraverty[1,*]

[1]*Institute of Nano Science and Technology, Phase-10, Sector-64, Mohali, Punjab 160062, India*

[2]*Indian Institute of Science Education and Research Mohali, Knowledge City, Sector-81, SAS Nagar, Manauli 140306, India*

(Received 13 October 2016; revised manuscript received 20 July 2017; published 13 September 2017)

Oxygen vacancies play an important role in controlling the physical properties of a perovskite oxide. We report alterations in the electronic properties of a cubic perovskite oxide, namely, $KTaO_3$, as a function of oxygen vacancies. The conducting surface of the $KTaO_3$ single-crystal substrate has been realized via Ar^+ irradiation. The band gap changes as a function of conductivity which is controlled by irradiation time, indicating the formation of defect states. Kelvin probe force microscopy suggests a sharp increase in the work function upon Ar^+ irradiation for a short period of time followed by a monotonic decrease, as we increase the irradiation time. Our experimental findings along with theoretical simulations suggest a significant surface dipole contribution and an unusual change in the electronic band line-up of $KTaO_3$ due to oxygen vacancies.

DOI: 10.1103/PhysRevB.96.115423

Recently, oxides have been gaining an unrivalled position in the field of spintronics based applications because of their broad spectrum of properties like ferroelectricity, ferromagnetism, charge ordering, etc. The first and the most well-known proposed spintronics device is the Datta-Das transistor, where the magnetic spin precession of a relativistic electron is controlled via external electric field perpendicular to the conduction electron plane [1,2]. Momentum-dependent splitting of the spin band in an electronic system, the Rashba effect, is a prerequisite to realize such a spin field-effect transistor [3]. The essential condition for Rashba effect is strong spin-orbit coupling. Giant Rashba-type spin splitting has already been observed in bulk layered polar semiconductor BiTeI with broken inversion symmetry [4].

Realizing Rashba effect in a simple cubic perovskite (ABO_3) will have added advantage because of two major factors. First, the simple cubic structure of perovskite oxides gives the opportunity to realize high-quality interface and superlattice structures. Second, perovskite oxides host a variety of interesting properties such as superconductivity, ferroelectricity, ferromagnetism, etc., hence these properties can also be integrated to the Rashba effect to achieve emergent phenomena if a suitable interface and/or superlattice is designed [5–8].

Among all perovskite oxides, semiconducting $SrTiO_3$ (STO) has attracted much attention in terms of realization of a two-dimensional electron gas (2DEG) system because of high electron mobility ($\sim 10^4$ cm^2 V^{-1} s^{-1}) [9,10]. However, in achieving low-dimensional electron gas, there is always a possibility of creating oxygen vacancies. The oxygen vacancies play a crucial role in the modification of surface composition, band structure, and hence transport properties of the conducting electrons in the system. The creation and effect of oxygen vacancies on the physical properties of STO have been studied in detail [11].

The other promising perovskite oxide to achieve low-dimensional electron gas is $KTaO_3$ (KTO), which is known to have electron mobility comparable to STO ($\sim 10^4$ cm^2 V^{-1} s^{-1}) [12]. In comparison to STO, however, KTO has an added advantage of having stronger spin-orbit coupling due to the *5d* Ta atom which enhances the Rashba effect as opposed to *3d* or lower orbitals in STO. Low-dimensional electron gas has been achieved in KTO single crystals by both liquid and solid-state gating as well as through ion bombardment [6,12,13]. However, the effect of oxygen vacancies on electronic properties of KTO has not been explored in detail.

In this paper, we have realized the electron conducting surface of KTO by creating oxygen vacancies through Ar^+ bombardment. The sheet charge-carrier density was systematically varied by changing the Ar^+ bombardment time. Combining optical spectroscopy and Kelvin probe force microscopy (KPFM), we have seen the appearance of defect states and an anomalous change in work function as a function of oxygen vacancies vis-à-vis charge-carrier densities. With the experimental measurements, density functional theory (DFT) based calculations on the bulk KTO and KTO slab have been performed to understand the electronic structure and electron distribution of the KTO surface as a function of oxygen vacancy. Our calculations reveal a strong and nontrivial correlation between oxygen vacancy, surface dipole, and charge distribution in KTO.

First-principles electronic structure calculations have been carried out to understand the nature of the electronic charge carriers in KTO. Figure 1(b) shows the projected density of states of constituent atoms of KTO. Figure 1(c) further resolves the orbital character of the conducting electrons into "Ta" atom basis states, which suggests clearly that conduction electrons of KTO possess mainly "Ta" *5d* electronic character. This is in good agreement with the case of STO, which had a strong "Ti" *3d* electronic character in its conduction electrons as reported by Henrich *et al.* [11]. This is a crucial point for the choice of KTO for the present paper, since the presence of *5d* character in conduction electrons is important for spin-orbit coupling.

We bombarded the KTO (001) single crystals with Ar^+ ions for different durations of time using the reactive ion etch mode in the SI500 system (Sentech) at 80-mtorr pressure, −530 V bias voltage, rf power of 225 W, and flow rate of 100 SCCM of Ar (initially, the system was kept under high vacuum for 1 h and

*suvankar.chakraverty@inst.ac.in

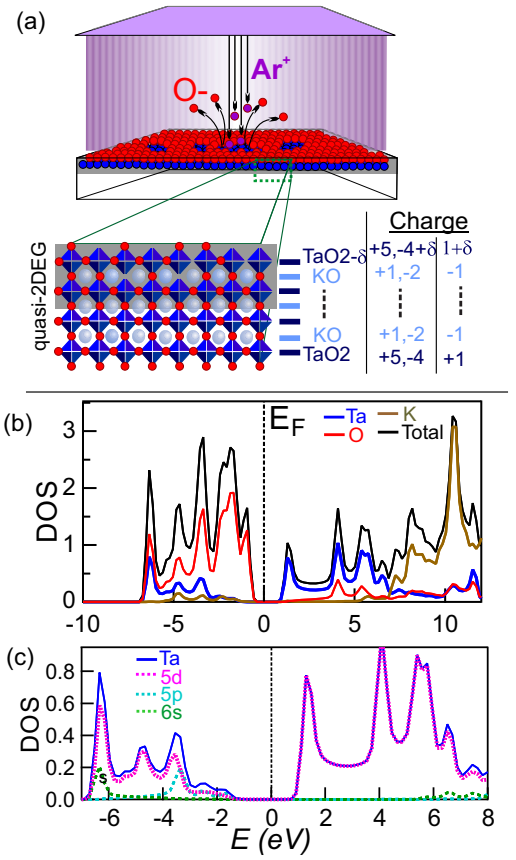

FIG. 1. (a) Schematic diagram of Ar^+ irradiation of KTO single crystals and possible formation of quasi-2DEG due to oxygen vacancies. The lower left panel shows the crystal structure of KTO near and away from the surface. The next panel shows the atomic arrangements at different layers. The right panel shows the charge distribution at each layer and formation of the *n*-doped surface. Colored lines in (b) represent the DOS of individual Ta, O, and K atoms. (c) DOS of *5d*, *5p*, and *6s* orbitals of Ta along with total DOS of Ta are shown, clearly manifesting *5d* orbital electrons across the conduction band.

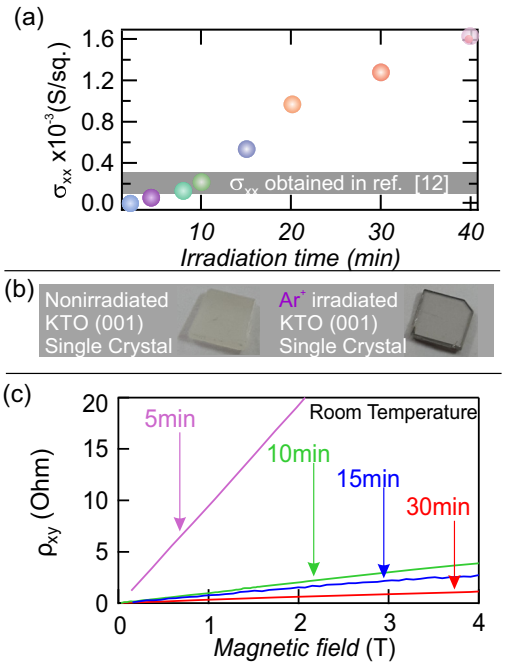

FIG. 2. (a) Room-temperature sheet conductance as a function of irradiation time. The gray area indicates the values of room-temperature sheet conductance reported in Ref. [12]. (b) Optical image of nonirradiated (left) and Ar^+ irradiated (right) KTO. (c) Hall resistance measurements of Ar^+ irradiated samples at room temperature. Linearity of the curves suggests the presence of a single type of charge carriers (electrons in our case).

was subsequently conditioned with Ar^+ for another 1 h). The bias voltage was enough to strip oxygen from surface levels [12]. In semiconductor accumulation layers or inversion layers like in metal oxide semiconductor (MOS) structures, the total charge is given by $Q = C[V - V_T]$, where C is the geometric capacitance of the MOS structure. The V_T depends on the band gap as well as impurities that produce localized states [14,15]. The exposure time in the present case is analogous to the applied voltage, increasing the effective charge-carrier density. The bombardment energy corresponding to this bias voltage gives rise to a penetration depth of around 15 nm as calculated from

$$L = 1.1\frac{E^{2/3}W}{\rho\left(Z_i^{1/4} + Z_t^{1/4}\right)^2}$$

where E is the energy of Ar^+ in eV, W is the atomic weight of the target in atomic mass units, ρ is the target specific gravity, and $Z_{i,t}$ are the atomic numbers of the ion and target, respectively [16]. This suggests the formation of a quasi-2DEG system of ~10-nm thickness. The time of bombardment was varied from 2 to 40 min keeping other parameters the same. A systematic increase in sheet conductance of the samples was observed with increasing bombardment time and all the samples were found to be conducting down to 2 K. The irradiation process and possible scenario of oxygen vacancies in KTO crystal upon irradiation are schematically shown in Fig. 1(a). After bombardment, the crystals turned grayish black as seen in Fig. 2(b). Oxygen vacancies in bulk KTO may also be created by using high-temperature annealing as reported for STO [17]. The Ar^+ bombardment method in the present case was adopted over high-temperature annealing in vacuum because potassium is a volatile material and high-temperature annealing may create potassium vacancies as well. Ar^+ irradiation might have also caused potassium vacancies in the system. To check this possibility, we annealed all the bombarded samples in air at 400 °C for 4 h, and all conducting samples turned insulating. This suggests that the appearance of conductivity is due to oxygen vacancies. On increasing the irradiation time from 2 to 40 min, there is an increase in the charge-carrier density from 1.3×10^{13} to 1.7×10^{15} cm^{-2} and hence the conductance increases by almost two orders of magnitude as observed in Fig. 2(a).

Optical spectroscopy had been performed on all the samples using an Agilent Carry UV-Vis-NIR spectrometer. Transmission spectra in Fig. 3(a) show percentage decrease in the transmission of light on increasing the irradiation time, indicating the increase in free charge carriers in the system. It was also observed from the transmission spectra that there

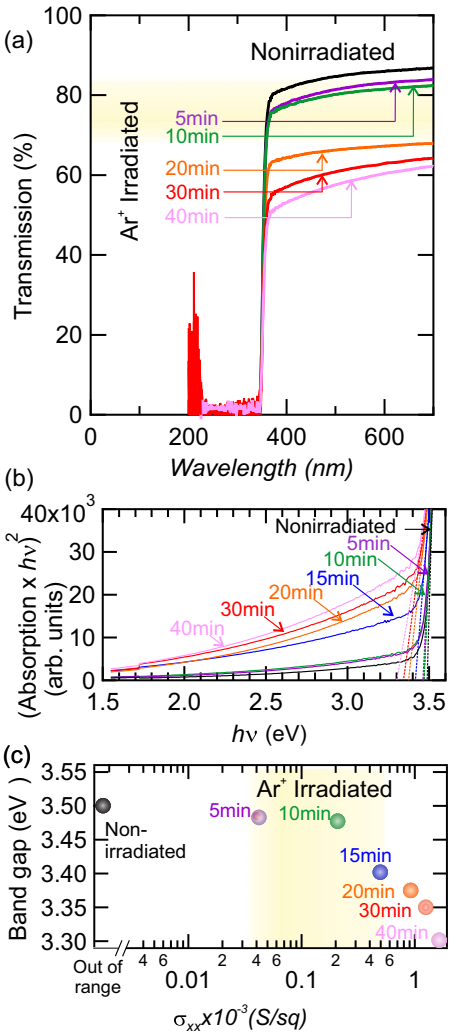

FIG. 3. (a) Optical transmission data of Ar^+ irradiated and nonirradiated KTO single crystals. (b) (Optical absorption $\times$ $h\nu)^2$ as a function of photon energy is plotted to estimate the band gap. Dotted lines are tangents to determine the band gap. (c) Band gap of KTO single crystals as a function of room-temperature sheet conductance.

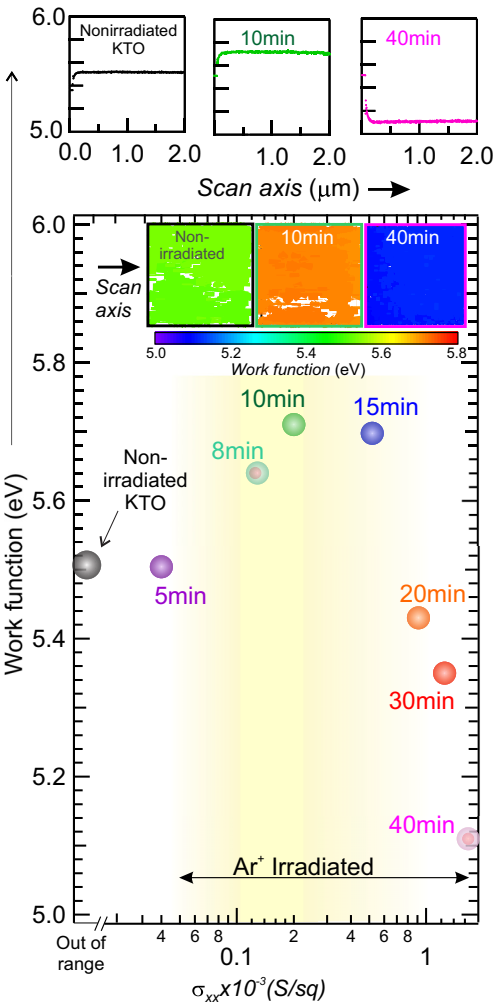

FIG. 4. The top panel shows the average work function of the nonirradiated, 10-min and 40-min irradiated samples as a function of scan length. The bottom panel shows the work function of KTO single crystals as a function of sheet conductance at room temperature measured by KPFM. The inset shows contour plots of the work function of nonirradiated, 10-min and 40-min irradiated samples. The color bar below indicates the work function in eV.

were roughly two regions of percentage transmission. Up to 10 min of irradiation, change in the percentage transmission is small while there is a sudden change after that. Similar behavior has been observed in the case of the optical band gap. The optical band gap has been estimated from the tangent of the (absorption $\times$ incident photon energy)^2 curve as a function of incident photon energy ($h\nu$) [Fig. 3(b)]. In Fig. 3(c), we have plotted the band gap as a function of sheet conductivity that also indicates two irradiation regions: slightly irradiated (up to 10 min) and heavily irradiated (above 10 min), respectively. From this observation, we infer that during the initial irradiation process free charge carriers are generated that increase the absorption of photons even with lower energies. Further bombardment generates electronic states at the conduction-band (CB) edge, decreasing the band gap.

To estimate the overall changes in the surface potential upon bombardment for different durations of time, KPFM was performed using a Bruker Multimode 8 AFM [18–20]. For KPFM, we used a conducting tip (tip model: SCM-PIT) and calibrated its work function using gold as the standard sample the work function of which is known to be 5.1 eV. On knowing the work function of the tip, we measured the contact potential difference (CPD) between the tip and the samples. The work function of the tip and the CPD were then used to calculate the work function of our samples. The contour plots of the work function of nonirradiated, 10- and 40-min irradiated samples for a 2 $\times$ 2-μm region are shown in Fig. 4 (inset). The color bar below indicates the work function of the samples. The average work functions of these samples along the scan length are shown in Fig. 4 (top panel). A nonmonotonic change in the work function of the irradiated KTO samples was observed as a function of conductivity vis-à-vis irradiation time as depicted in Fig. 4. The expected decrease in the work function for an electron doped system was preceded by an

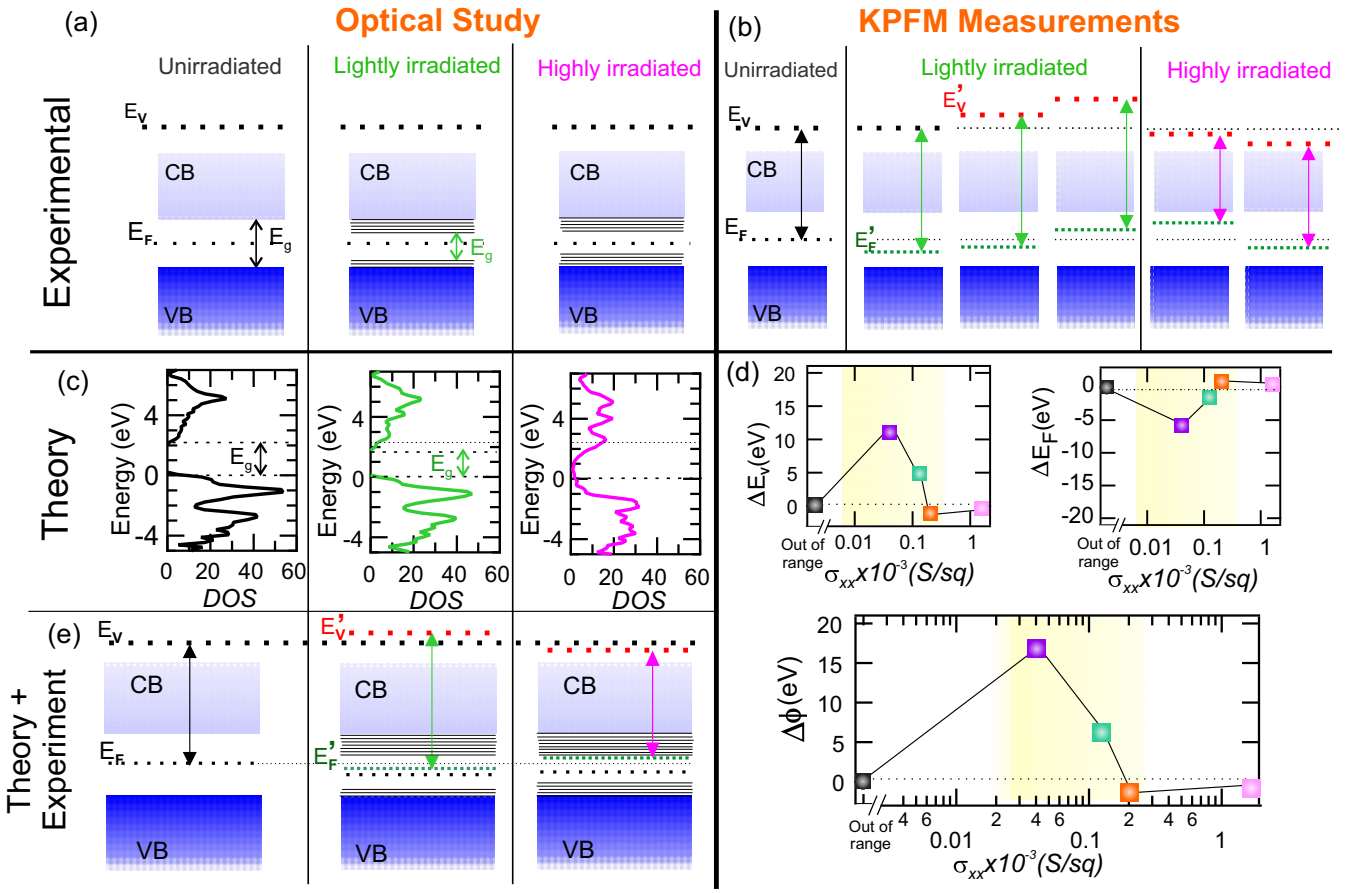

FIG. 5. (a) and (b) Depiction of possible band-structure modifications taking place according to experimental optical spectroscopy and KPFM measurements, respectively. (c) DOS of unirradiated (left), lightly irradiated (middle), and highly irradiated (right) KTO calculated from first-principles DFT calculations. (d) Change in vacuum level (top left), Fermi level (top right), and work function (bottom) calculated from surface-potential calculations by including the oxygen vacancies. (e) Band diagrams for unirradiated, lightly irradiated, and highly irradiated samples obtained by combining experimental observations and theoretical calculations.

initial increase in it, suggesting the possibility of two kinds of charge carriers (electrons and holes) in the system. To verify this, Hall measurements were done using a Quantum Design physical property measurement system (PPMS). Linear curves of Hall resistance as a function of magnetic field in Fig. 2(c), however, clarified the existence of only one type of charge carriers. Similar to optical data, two distinct regions were seen in the KPFM plot. Up to 10 min of bombardment, there was an anomalous increase in work function, while above 10 min the work function monotonically decreased as expected. All the measurements on bombarded samples were done immediately after bombardment to avoid aging effect.

Figures 5(a) and 5(b) show the illustrated depiction of the possible band-structure modifications taking place according to the experimental results. Figure 5(a) shows the band diagrams for the unirradiated, lightly irradiated, and highly irradiated KTO samples where the band gap decreases on increasing the bombardment time. Optical property measurements shown in Fig. 3(c) suggest that with short irradiation time there is a small change in band gap, followed by a sharp decrease in it with further increase in irradiation time. Accordingly, our middle band diagram [Fig. 5(a)] mimics this situation through the introduction of defect states between conduction band and valence band (VB). Figure 5(b) shows the possible band line-up of the unirradiated and irradiated samples based on our KPFM observations. Figure 5(b) (middle) shows several possible band-structure reconstructions that can explain the increase in work function as we have seen for lightly irradiated samples. We have shown the three most probable scenarios: (i) movement of the Fermi level (E_F) towards the VB with no change in vacuum level (E_V), (ii) movement of E_F towards the VB as well as movement of E_V away from the CB, and (iii) movement of E_F towards the CB accompanied by a larger shift of E_V away from the CB. For highly irradiated samples we have presented two of the possible cases where we show that the decrease in work function can be due to (i) movement of E_F towards the CB accompanied by shifting of E_V downwards or (ii) movement of E_F towards the VB along with a larger downward shift of E_V.

To identify the band structure as a function of oxygen vacancies out of these several possible combinations, DFT based theoretical band-structure calculations have been performed [21–24]. Here, we used the Perdew-Burke-Ernzerhof [25] exchange-correlation functional and projector augmented wave basis set as implemented in the Vienna Ab Initio Simulation Package [26,27] to calculate the DOS and work function of the KTO slab. For the bulk cubic unit cell of the KTO, a $4 \times 4 \times 4$ Gamma centered K mesh was used.

The surface of KTO was constructed as a two-dimensional slab by considering periodic boundary conditions along x and y directions and a 20-Å vacuum region separating two repeating regions along the z (001) direction. Two-dimensional slab geometry of thickness 15.9 Å has been created with a $2 \times 2 \times 4$ supercell of 80 atoms. The (001) surface of KTO was studied in this present calculation. For oxygen vacancy calculation, 4.1, 20.8, 37.9, and 50% of oxygen vacancy is created in the supercell. It is found that oxygen vacancy creates an electron donating point defect in the structure [see Fig. 5(c)]. Figure 5(c) shows the DOS for unbombarded (no oxygen vacancies), slightly bombarded (4.1% oxygen vacancies), and heavily bombarded (20.8% oxygen vacancies) systems. This figure suggests the DOS as well as band gap remain similar (very small reduction) with slight bombardment in comparison to the unbombarded system whereas the band gap significantly collapses for the heavily bombarded system. This calculation further strengthens our claims based on experimental (optical) observations.

To understand the nonmonotonic behavior of the work function ($\phi = E_V - E_F$) as a function of oxygen vacancies and identify the possible band line-up out of several possibilities shown in Fig. 5(b), we have theoretically calculated change in vacuum level (ΔE_V), Fermi level (ΔE_F), and work function ($\Delta\phi$) as a function of oxygen vacancy [Fig. 5(d)]. These values have been extracted from the theoretical calculations performed on the 2D KTO slab. We have considered a finite thickness of the 2D KTO for the work function and vacuum level calculations. Due to this finite size, there might be a quantum size effect error [28]. These calculations show a significant effect of surface dipoles with oxygen vacancies, leading to an anomalous change in vacuum level as well as Fermi level. The work function extracted from the calculations as a function of oxygen vacancy shows qualitatively very similar nonmonotonic behavior [Fig. 5(d)] as observed experimentally. Combining all the results of theoretical simulations with our experimental observations, we have proposed the band line-up of lightly and heavily irradiated samples in Fig. 5(e). Upon light bombardment, E_F moves downwards due to formation of localized defect states near the CB and band-gap modifications. Also, there is an upward shift in E_V due to surface reconstruction. In case of highly bombarded samples, there is an upward movement of E_F indicating the n type of charge carriers in the system and E_V also moves slightly downwards as shown in Fig. 5(e). The theoretical estimates from DFT overestimate the work function but qualitatively models a trend of nonmonotonous behavior. This discrepancy is a result of the finite-size effect of the DFT. The oxygen vacancy profile created by Ar^+ bombardment has an estimated depth of ~15 nm whereas we had performed the density functional theory calculation on a 2D slab geometry of thickness 1.59 nm and a $2 \times 2 \times 4$ supercell with 80 atoms. A rudimentary model such as ours does not incorporate other minor perturbations like structural distortions or surface reconstruction. Overall the theoretical estimates of both the vacuum level and Fermi level of defected 2D structures are affected by the finite-size effect. The data and theoretical estimates make it an interesting system to study surface reconstruction and structural distortion using techniques like scanning tunneling microscopy and high-resolution transmission electron microscopy.

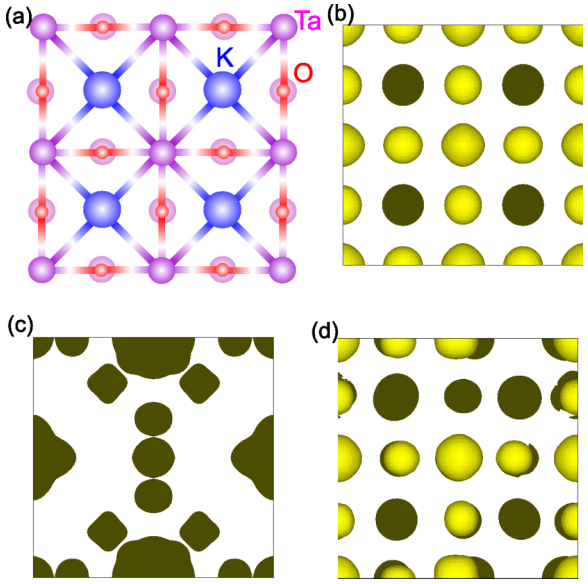

FIG. 6. (a) Top view of the (0 0 1) surface of KTO. (b), (c), and (d) present the electronic charge distribution of unirradiated, lightly irradiated, and highly irradiated KTO samples, respectively, where yellow color represents positive charge and dark green color represents negative charge.

To further investigate this nontrivial behavior in the work function, we have also plotted the charge-density isosurface (see Fig. 6). Figure 6(a) shows the top view of the (0 0 1) surface of KTO and Figs. 6(b)–6(d) represent the charge density of the pure KTO slab, the 4.1% oxygen vacant slab, and the 20.8% oxygen vacant slab. The yellow and green color isosurfaces correspond to positive and negative values, respectively. An interesting pattern is found in the charge-density plot for these vacancies. In the pure slab, charge density is equivalently distributed on all surface atoms. For the 4.1% vacancy, positive charge is completely depleted and charge density is very localized. However, the positive charge isosurface has a strong presence on the 20.8% oxygen vacant slab [Fig. 6(d)] and the charge distribution is very similar to the unbombarded KTO slab. Depletion of charge density at 4.1% vacancy increases the dipole moment of the surface, and plausibly the high dipole moment plays a crucial role to increase the vacuum potential and hence the work function at low percentage vacancy, while smoothing of electron charge density for a higher percentage vacancy decreases the dipole moment and hence the work function [29].

In conclusion, the oxygen vacant electron doped conducting surface of KTO has been prepared via Ar^+ irradiation. Density functional theory indicates that these conduction electrons have Ta *5d* character and could be a good hunting ground for Rashba effect. Optical spectroscopy along with KPFM measurement clearly indicate two distinct effects of irradiation, where in the initial slight irradiation process (up to 10 min in our case) a small change in band gap with an anomalous change in work function has been observed. Longer exposure to Ar^+ produces a sharp decrease in band gap with a usual monotonic

decrease in work function as a function of increasing irradiation time vis-à-vis charge-carrier density. DFT calculations suggest a significant effect of the surface dipole and modification of the electronic DOS, especially a nontrivial change in vacuum level due to oxygen vacancies upon Ar^+ irradiation.

S.C. and A.V. acknowledge financial support from Department of Science and Technology (DST), India Nano Mission Projects No. SR/NM/NS-1007/2015 and No. SR/NM/NS-11098/2011, respectively. A DST (India) Ramanujan Fellowship is gratefully acknowledged. M.S. would like to acknowledge financial support from DST (India) Science and Engineering Research Board Project No. PDF/2016/001227. C.B. and A.D.S. remain highly thankful to Centre for Development of Advanced Computing, Pune for providing its supercomputing facilities on PARAM-YUVA-II. Also, the authors would like to acknowledge Dr Y. Singh for access to physical property measurement system facility at IISER Mohali.

[1] S. Datta and B. Das, Appl. Phys. Lett. **56**, 665 (1990).
[2] T. Matsuyama, C.-M. Hu, D. Grundler, G. Meier, and U. Merkt, Phys. Rev. B **65**, 155322 (2002).
[3] Y. A. Bychkov and E. I. Rashba, Pis'ma Zh. Eksp. Teor. Fiz. **39**, 66 (1984) [JETP Lett. **39**, 78 (1984)].
[4] K. Ishizaka, M. S. Bahramy, H. Murakawa, M. Sakano, T. Shimojima, T. Sonobe, K. Koizumi, S. Shin, H. Miyahara, A. Kimura, K. Miyamoto, T. Okuda, H. Namatame, M. Taniguchi, R. Arita, N. Nagaosa, K. Kobayashi, Y. Murakami, R. Kumar, Y. Kaneko, Y. Onose, and Y. Tokura, Nat. Mater. **10**, 521 (2011).
[5] K. Ueno, S. Nakamura, H. Shimotani, A. Ohtomo, N. Kimura, T. Nojima, H. Aoki, Y. Iwasa, and M. Kawasaki, Nat. Mater. **7**, 855 (2008).
[6] K. Ueno, S. Nakamura, H. Shimotani H. T. Yuan, N. Kimura, T. Nojima, H. Aoki, Y. Iwasa, and M. Kawasaki, Nat. Nanotech. **6**, 408 (2011).
[7] O. Tikhomirov, H. Jiang, and J. Levy, Phys. Rev. Lett. **89**, 147601 (2002).
[8] J. S. Lee, Y. W. Xie, H. K. Sato, C. Bell, Y. Hikita, H. Y. Hwang, and C. C. Kao, Nat. Mater. **12**, 703 (2013).
[9] A. Ohtomo and H. Y. Hwang, Nature (London) **427**, 423 (2004).
[10] Y. Hotta, T. Susaki, and H. Y. Hwang, Phys. Rev. Lett. **99**, 236805 (2007).
[11] V. E. Henrich, G. Dresselhaus, and H. J. Zeiger, Phys. Rev. B **17**, 4908 (1978).
[12] S. Harashima, C. Bell, M. Kim, T. Yajima, Y. Hikita, and H. Y. Hwang, Phys. Rev. B **88**, 085102 (2013).
[13] H. Nakamura and T. Kimura, Phys. Rev. B **80**, 121308 (2009).
[14] T. Ando, A. B. Fowler, and F. Stern, Rev. Mod. Phys. **54**, 437 (1982).
[15] B. G. Streetman and S. K. Banerjee, *Solid State Electronic Devices*, 6th ed. (Phi Learning Private, New Delhi, India, 2009).
[16] D. W. Reagor and V. Y. Butko, Nat. Mater. **4**, 593 (2005).
[17] F. V. E. Hensling, C. Xu, F. Gunkel, and R. Dittmann, Sci. Rep. **7**, 39953 (2017).
[18] W. Melitz, J. Shen, A. C. Kummel, and S. Lee, Surf. Sci Rep. **66**, 1 (2011).
[19] C. Maragliano, S. Lilliu, M. S. Dahlem, M. Chiesa, T. Souier, and M. Stefancich, Sci. Rep. **4**, 4203 (2014).
[20] A. K. Henning, T. Hochwitz, J. Slinkman, J. Never, S. Hoffmann, P. Kaszuba, and C. Daghlian, J. Appl. Phys. **77**, 1888 (1995).
[21] B. J. Morgan and G. W. Watson, Surf. Sci. **601**, 5034 (2007).
[22] J. A. Enterkin, A. K. Subramanian, B. C. Russell, M. R. Castell, K. R. Poeppelmeier, and L. D. Marks, Nat. Mater. **9**, 245 (2010).
[23] M. Nolan, S. Grigoleit, D. C. Sayle, S. C. Parker, and G. W. Watson, Surf. Sci. **576**, 217 (2005).
[24] G. Henkelman, B. P. Uberuaga, D. J. Harris, J. H. Harding, and N. L. Allan, Phys. Rev. B **72**, 115437 (2005).
[25] J. P. Perdew, K. Burke, and M. Ernzerhof, Phys. Rev. Lett. **77**, 3865 (1996).
[26] P. E. Blochl, Phys. Rev. B **50**, 17953 (1994).
[27] G. Kresse and D. Joubert, Phys. Rev. B **59**, 1758 (1999).
[28] C. J. Fall, N. Binggeli, and A. Baldereschi, J. Phys.: Condens. Matter **11**, 2689 (1999).
[29] A. J. Bennett and C. B. Duke, Phys. Rev. **188**, 1060 (1969).